Magnetic Fluctuations and Accelerated Particles in Astrophysical Shocks

Andrei Bykov

Ioffe Institute & KITP

Collisionless Plasma Shocks

- In a rarefied hot cosmic plasmas the Coulomb collisions are not sufficient to provide the viscous dissipation of the incoming flow, and collective effects due to the plasma flow instabilities play a major role, providing the collisionless shocks, as it was first directly observed in the heliosphere in 60s.

Collisionless Plasma Shocks

- The thickness of collisionless shocks is usually by many orders of magnitude less than the Coulomb mean free path.

  Strong Magnetic field fluctuations observed in the shock ramp indicated that plasma instabilities are responsible for the supersonic flow relaxation

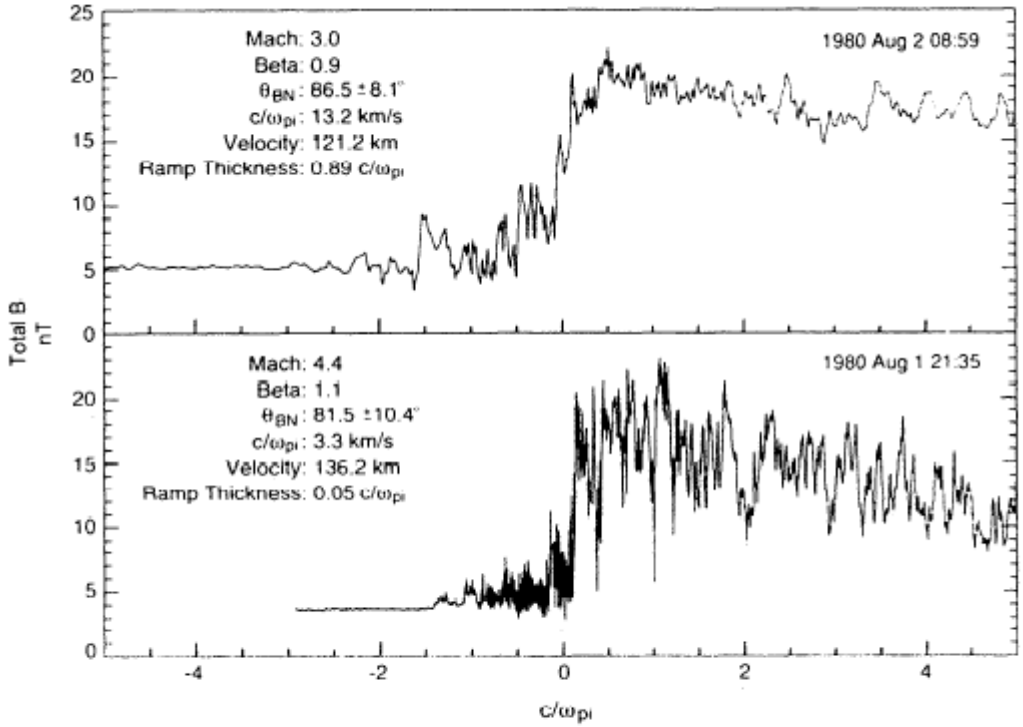

Figure 2. These shocks formed under similar solar wind conditions, but there is great disparity between their ramp widths.

IPM observations of quasi-transverse Collisionless Shocks

Newbury & Rusell 1996

Interplanetary Shock Turbulence

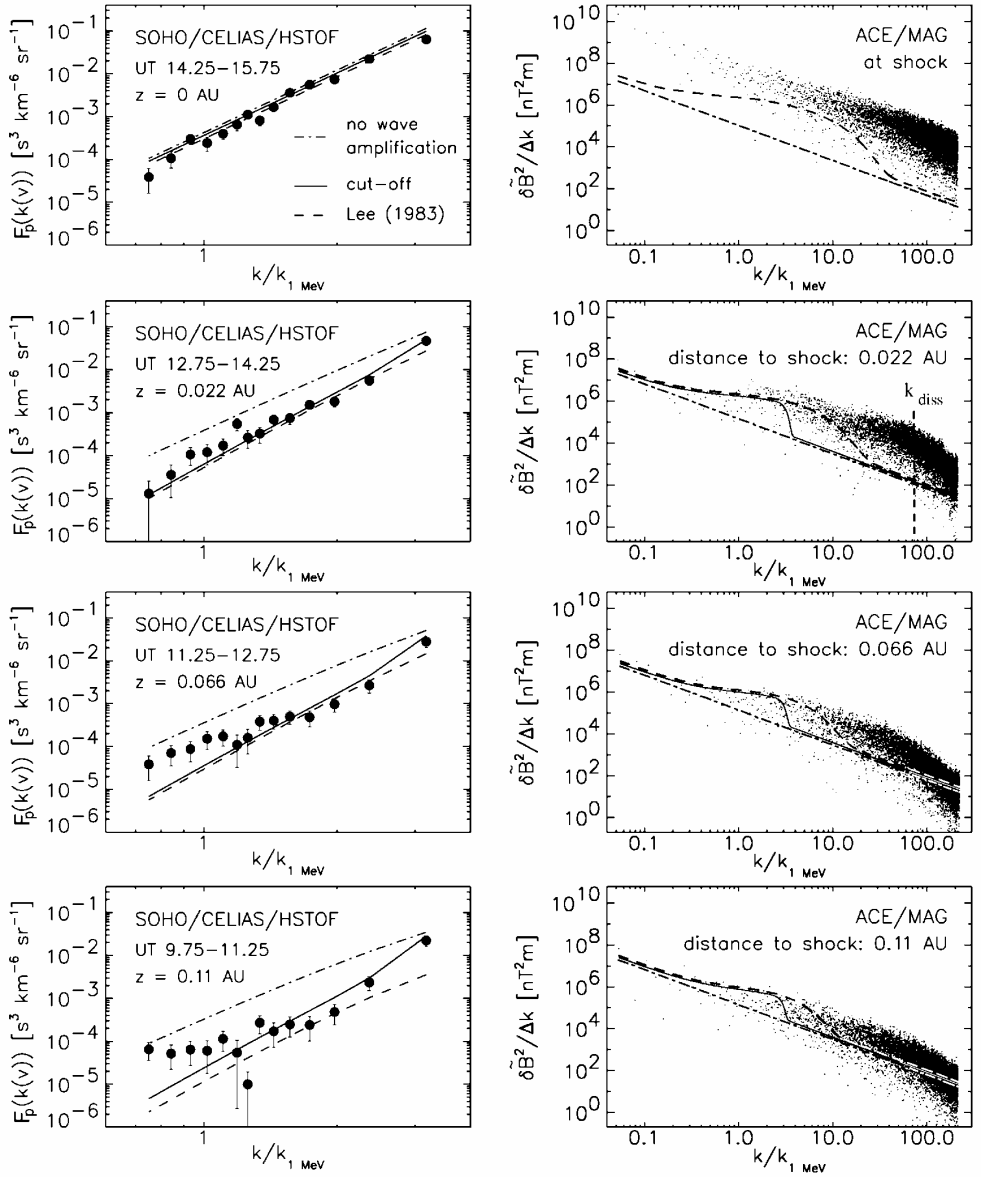

Bamert ea 2004

Collisionless Plasma Shock Simulations

- Particle-in-Cell Code simulations
- Hybrid Code Simulations

These are the most powerful tools to study the collisionless shock structure

on the scales of about a few thousands of proton gyro-radii

Hybrid simulation of a collisionless shock :

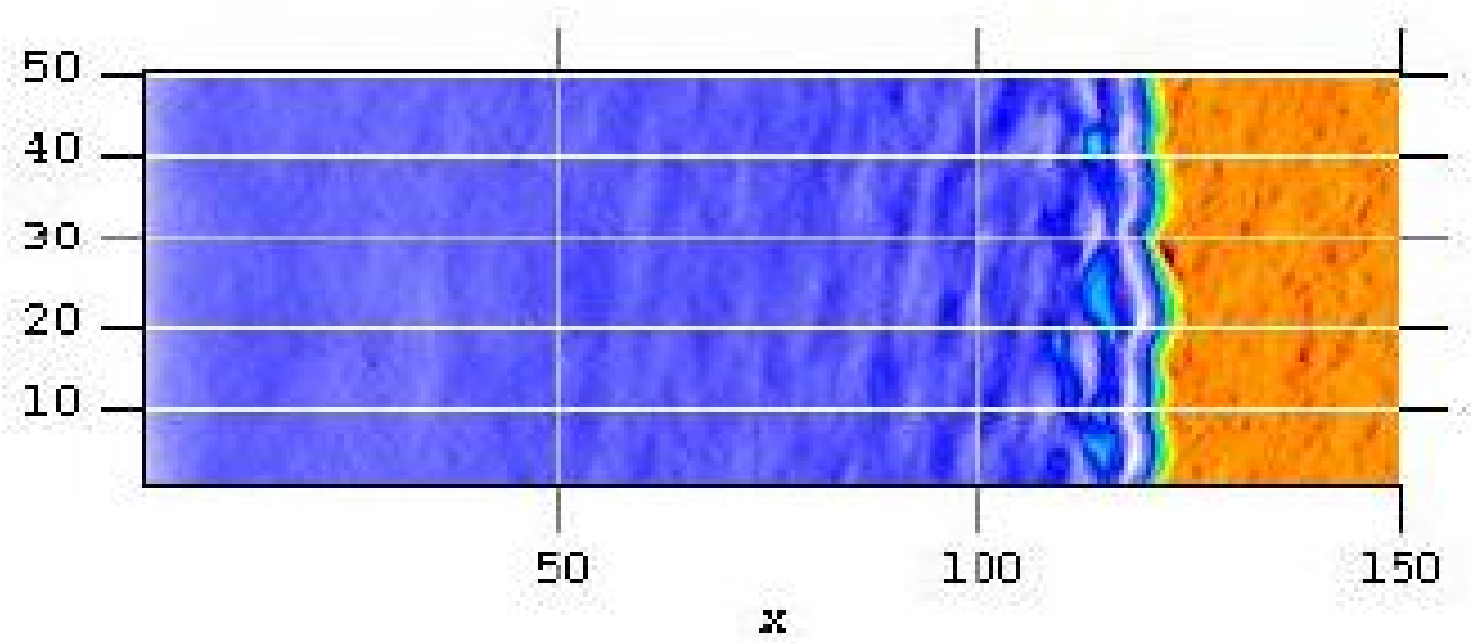

$$[x] = \frac{c}{\omega_{pi}} \sim 10^9 cm$$

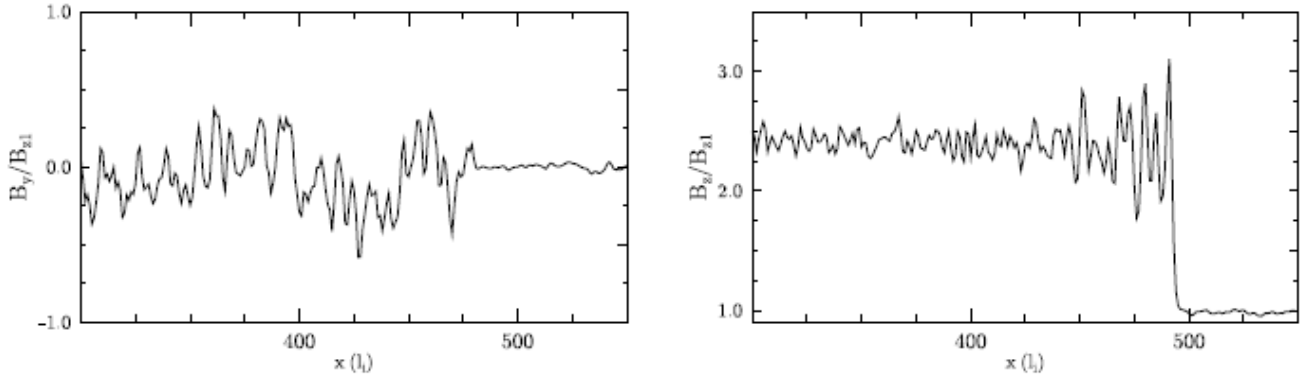

Fig. 2 Hybrid simulated magnetic fields of a quasi-perpendicular shock (80° inclination). The shock propagates along the x-axis, while the initial regular magnetic field is in the x–z plane. We show the B_y and B_z dependence on x in the left and right panels respectively.

Hybrid Simulations of a quasi-transverse Collisionless Shock

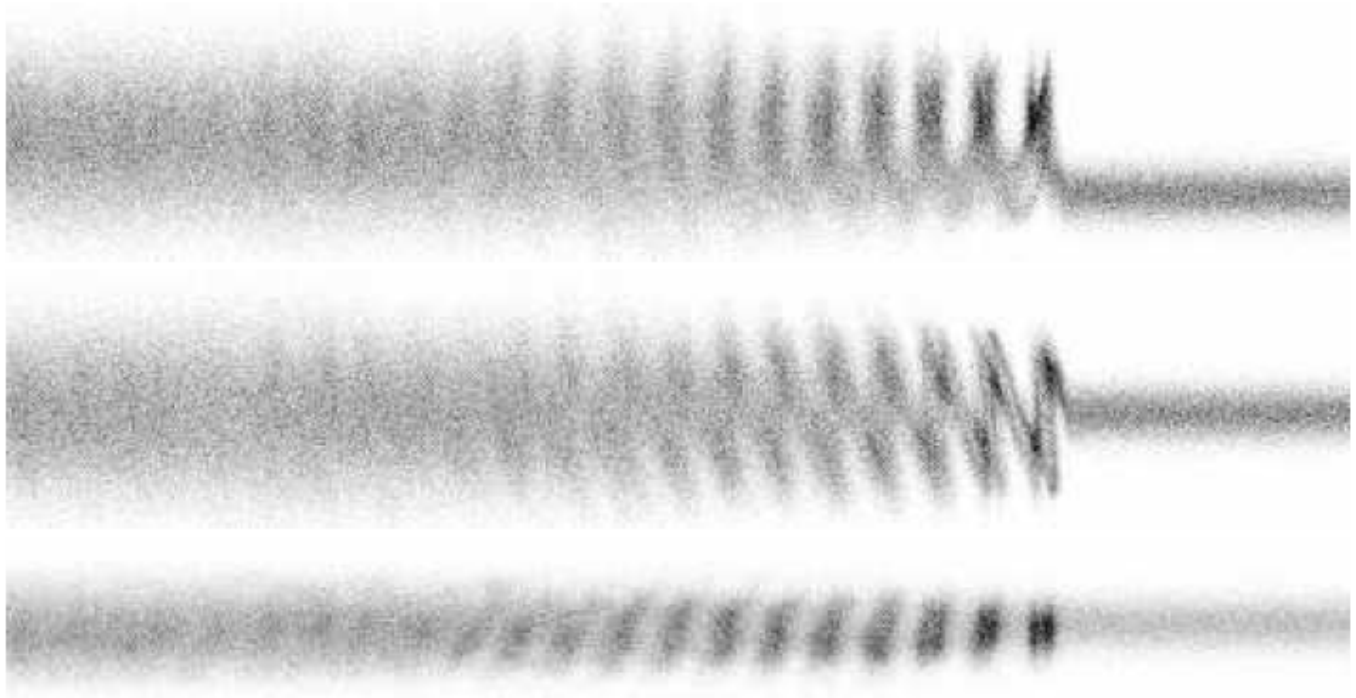

Fig. 1 O VII phase density in a hybrid simulated quasi-perpendicular shock (80° inclination). The shock is moving from left to right in the reference frame where the particle reflecting wall is at rest. The figures show the oxygen phase densities in $x - v_x$, $x - v_y$ and $x - v_z$ projections from top to bottom respectively. The size of the simulation box in x-dimension is about 300 l_{i}.

Hybrid Simulations of a quasi-transverse Collisionless Shock

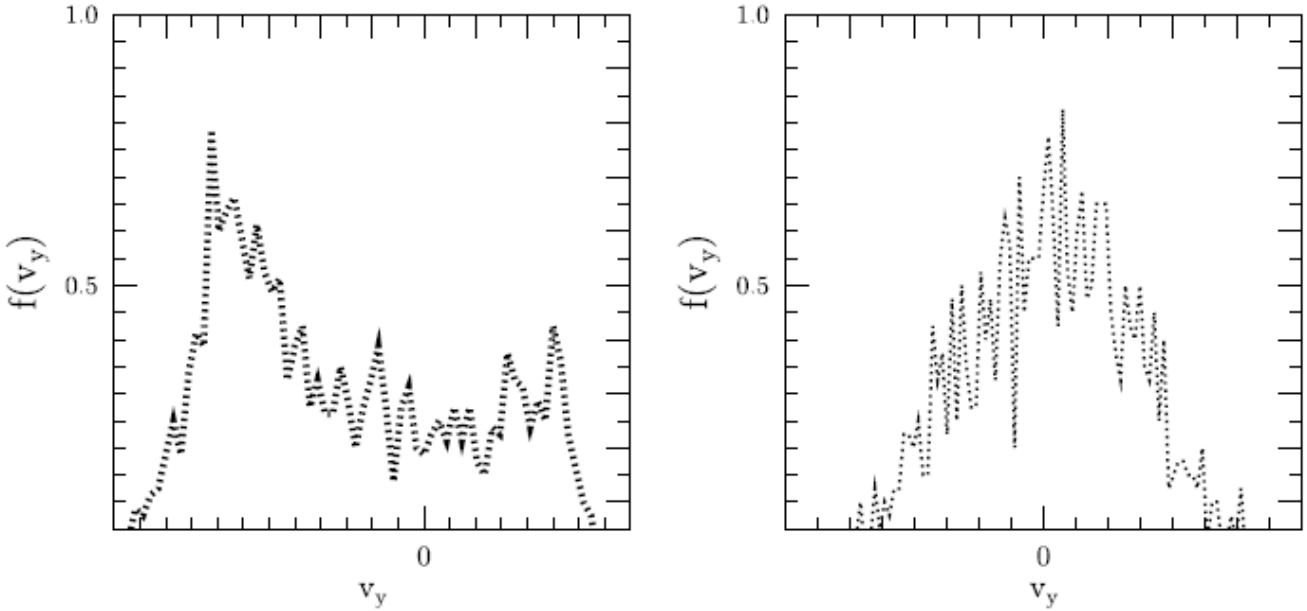

Fig. 2 Hybrid simulated O VII distribution function (normalised) as a function of a random velocity component $\delta v_y = v_y - < v_y >$ transverse to the downstream magnetic field in a quasi-perpendicular shock (80° inclination). The shock propagates along the x-axis, while the initial regular magnetic field is in the x–z plane. In the left panel the distribution in the viscous velocity jump is shown. The right panel shows the distribution behind the jump at the position of the left end in Fig. 1. Multi-velocity structure of the flow is clearly seen in the left panel, while it is relaxing to quasi-Maxwellian in the right panel.

Hybrid Simulations of a quasi-transverse Collisionless Shock

Diffusive Shock Acceleration

- In the course of the violent collisionless shock relaxation process some amount of particles may form a super-thermal population to be further accelerated to highly relativistic energies in extended cosmic shocks. Diffusive Shock Acceleration is the most popular scenario to do the job…

Diffusive Shock Acceleration

- the Diffusive Shock Acceleration to be efficient requires strong magnetic field fluctuations of scales many (more than 5) orders of magnitude larger than the ion inertial (and the shock width) … It can not yet be modeled in details by PIC or hybrid simulations

How computationally expensive the direct plasma simulations are?

$$\mathbf{N_x} \sim \frac{\kappa(E_{\rm max})/u_0}{(c/\omega_{pe})} \sim 6\times10^{11}\left(\frac{E_{\rm max}}{\rm TeV}\right)\left(\frac{u_0}{1000\,{\rm km\,s^{-1}}}\right)^{-1}\left(\frac{B}{\mu\rm G}\right)^{-1}\left(\frac{n_e}{\rm cm^{-3}}\right)^{1/2}\left(\frac{f}{1836}\right)^{1/2}, \quad \text{(A1)}$$

for the number of cells *in one dimension*. The factor $f = m_p/m_e$ is the proton to electron mass ratio. From the acceleration time condition, the required number of time steps is,

$$\mathbf{N_t} \sim \frac{\tau_{\rm acc}(E_{\rm max})}{\omega_{pe}^{-1}} \sim 6\times10^{14}\left(\frac{E_{\rm max}}{\rm TeV}\right)\left(\frac{u_0}{1000\,{\rm km\,s^{-1}}}\right)^{-2}\left(\frac{B}{\mu\rm G}\right)^{-1}\left(\frac{n_e}{\rm cm^{-3}}\right)^{1/2}\left(\frac{f}{1836}\right)^{1/2}. \quad \text{(A2)}$$

Even with $f = 1$ these numbers are obviously far beyond any conceivable computing capabilities and they show that approximate methods are essential for studying NL-DSA.

Too much...

Diffusive Shock Acceleration

- DSA in Non-relativistic shocks can not yet be modeled in full details by PIC or hybrid simulations…

  though there are nice PIC simulations of **relativistic** shocks by J.Arons, A.Spitkovsky and co-workers

Models of DSA

What can we do now?

- Kinetic models e.g. Axford ea (1977), Krimskii (1977, 1981), Bell (1978, 1987), Blandford and Ostriker (1978), Eichler (1979), Toptygin and co-workers, Drury and Volk, Berezhko and Volk, Blasi and co-workers, Ptuskin and Zirakashvili and many, many others…
- or just a non-linear gambling --- D.Ellison, F.Jones, M.Baring, and co-workers

Monte Carlo Model of DSA with Magnetic Turbulence Amplification in

Non-relativistic Shocks

Work done with D.C.Ellison and A.E.Vladimirov

MC model of DSA

- Particle scattering rate or MFP prescription (diffusion model)

- Magnetic Turbulence Model:

(i) Turbulence amplification and dissipation

(ii) Turbulence spectral transfer

Magnetic field amplification models:

Resonant models of wave generation

e.g. Wentzel (1969), Kulsrud & Cesarsky (1971), Skilling (1975), Achterberg (1981) and many others

Non-resonant models e.g. by Drury and Dorfi (1985) (long-wavelength CR pressure gradient instability), Bell (2004), Pelletier ea (2006) (a fast short-wavelength CR current instability). L –wavelength CR current instabilities by Bykov, Osipov, Toptygin (2005, 2009), Pelletier ea (2006), Reville et al (2007). L-wavelength instability by Malkov and Diamond and others

MC model of DSA

Two models of the turbulence spectral energy transfer

(i) Kolmogorov-type cascade

(ii) No-cascade in the mean-field direction

We used Bell's short wavelength instability as the magnetic field amplification mechanism

a fully nonlinear model* of DSA based on Monte Carlo particle transport

- Magnetic turbulence, bulk flow, super-thermal particles derived consistently with each other

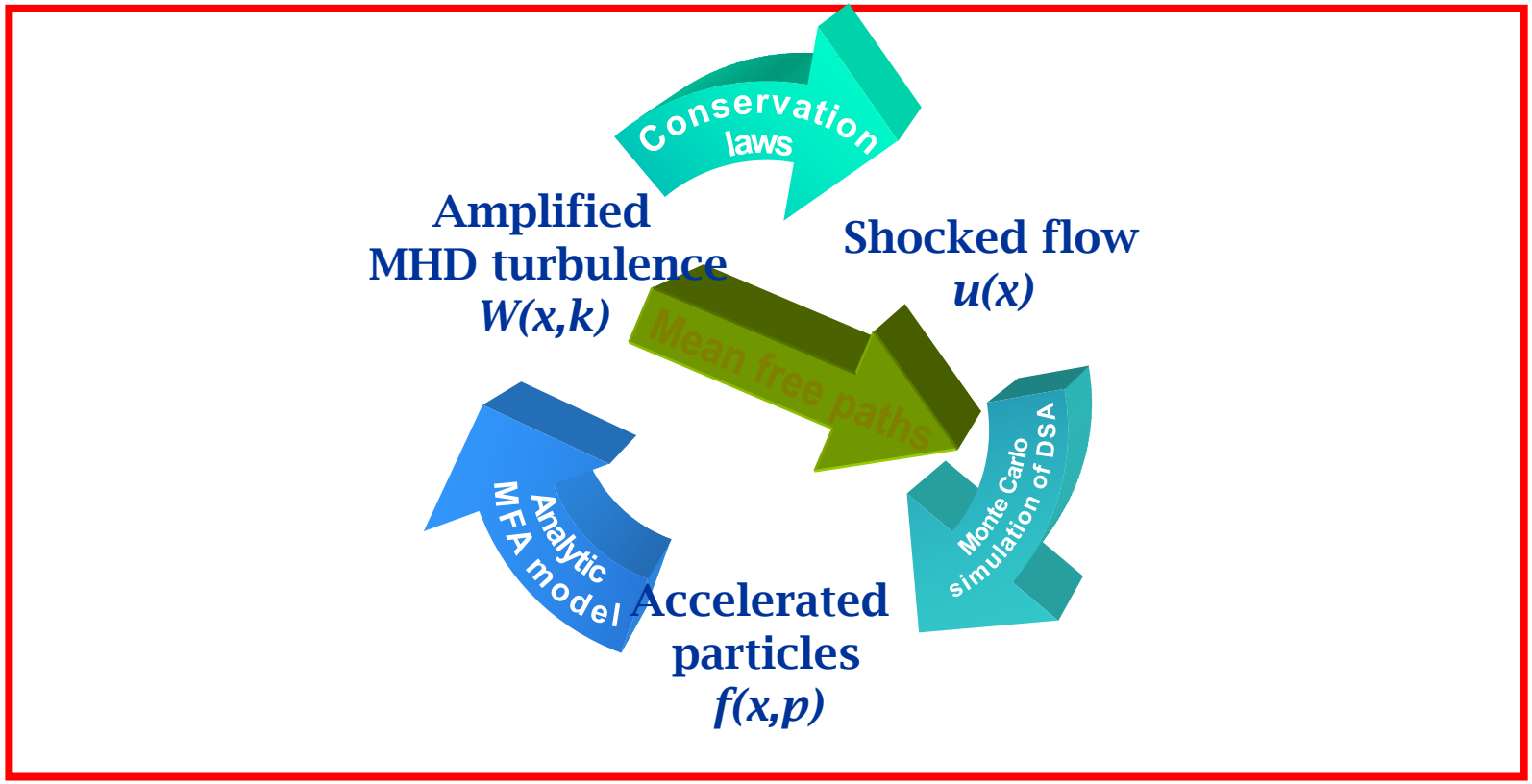

Vladimirov, Ellison & Bykov, 2006. ApJ, v. 652, p.1246;

Vladimirov, Bykov & Ellison, 2008. ApJ, v. 688, p. 1084

Vladimirov, Bykov & Ellison, 2009. ApJ, v. 703, L29

The Structure of Supersonic Flow

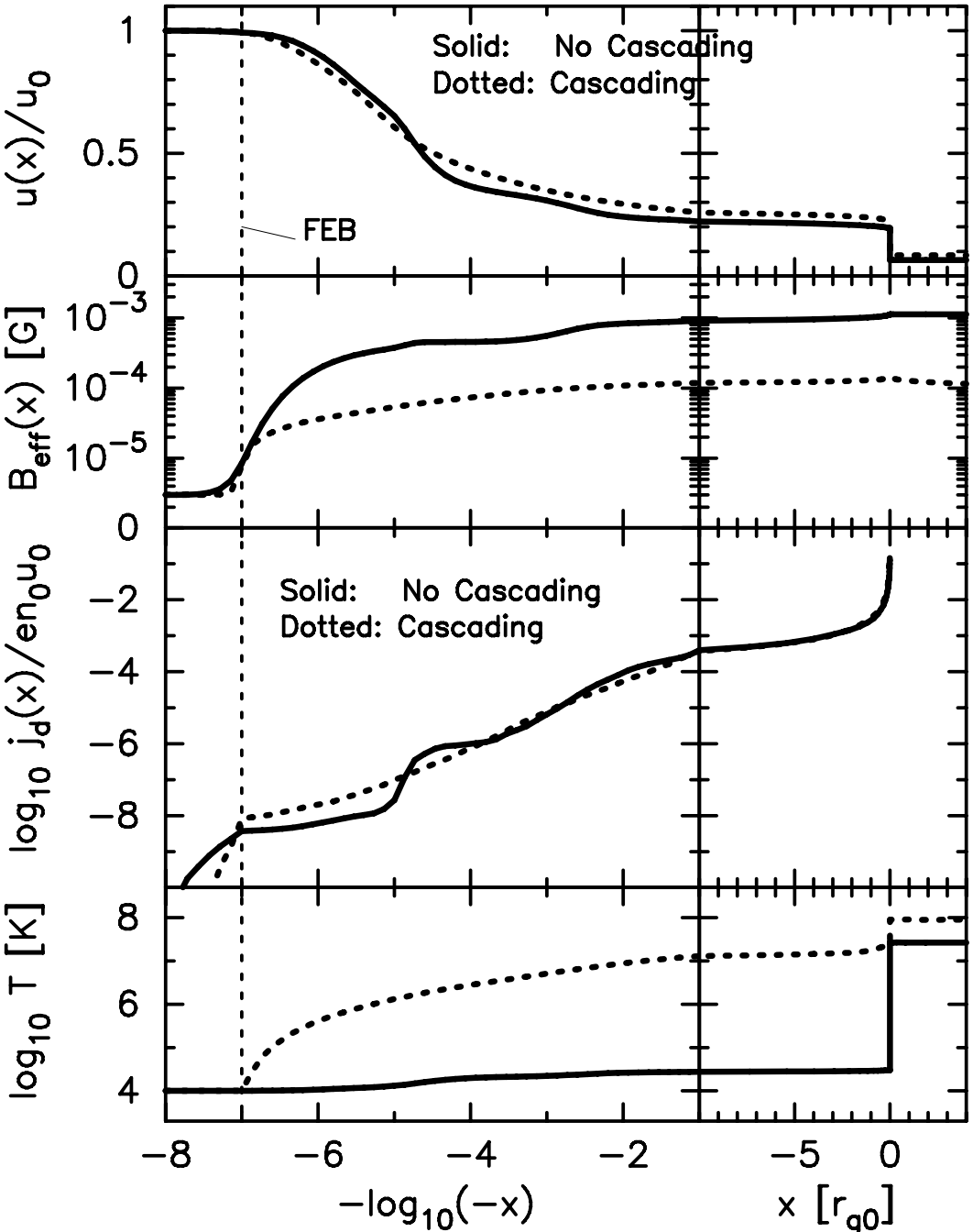

Magnetic Fluctuation Spectra

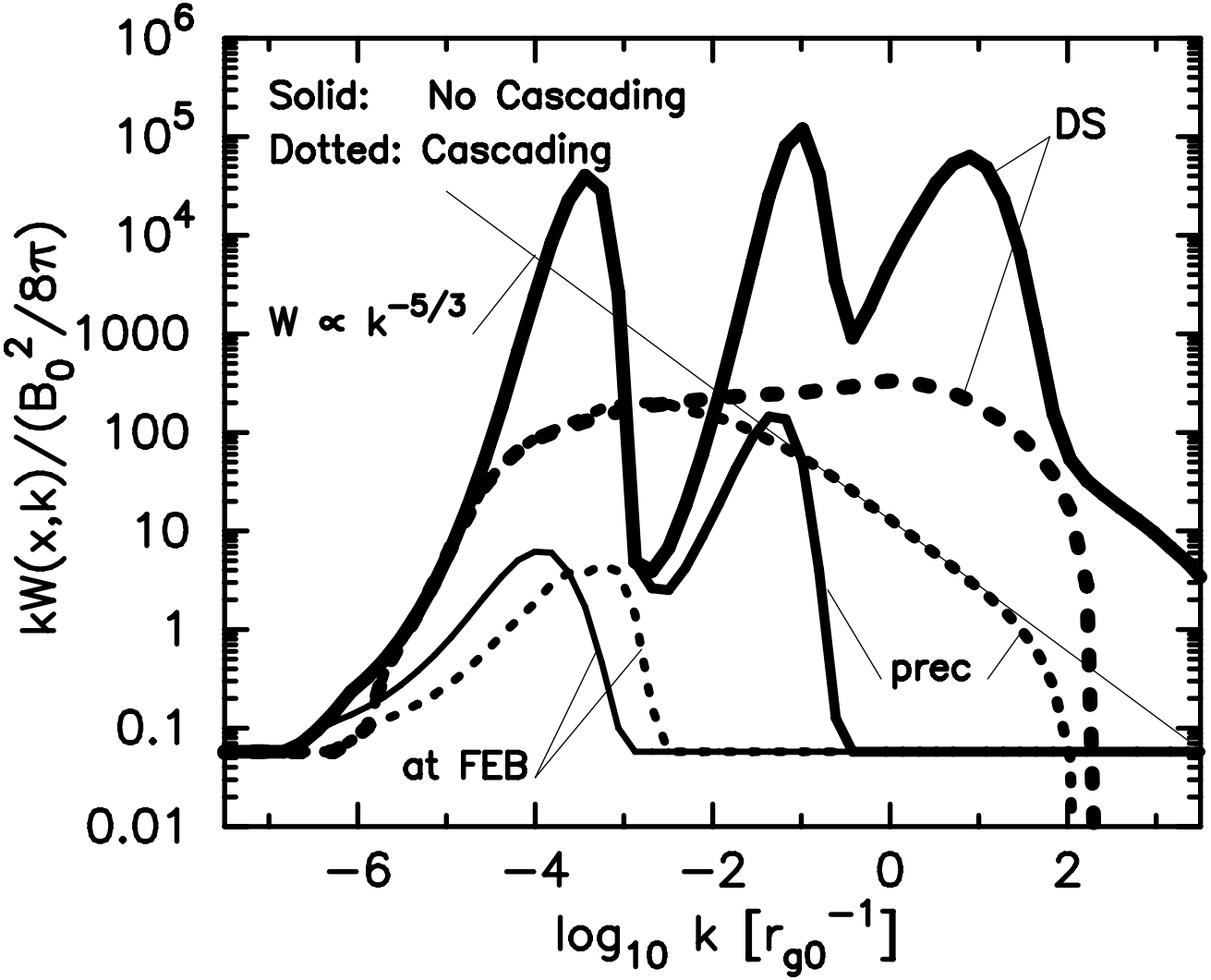

Particle Spectra

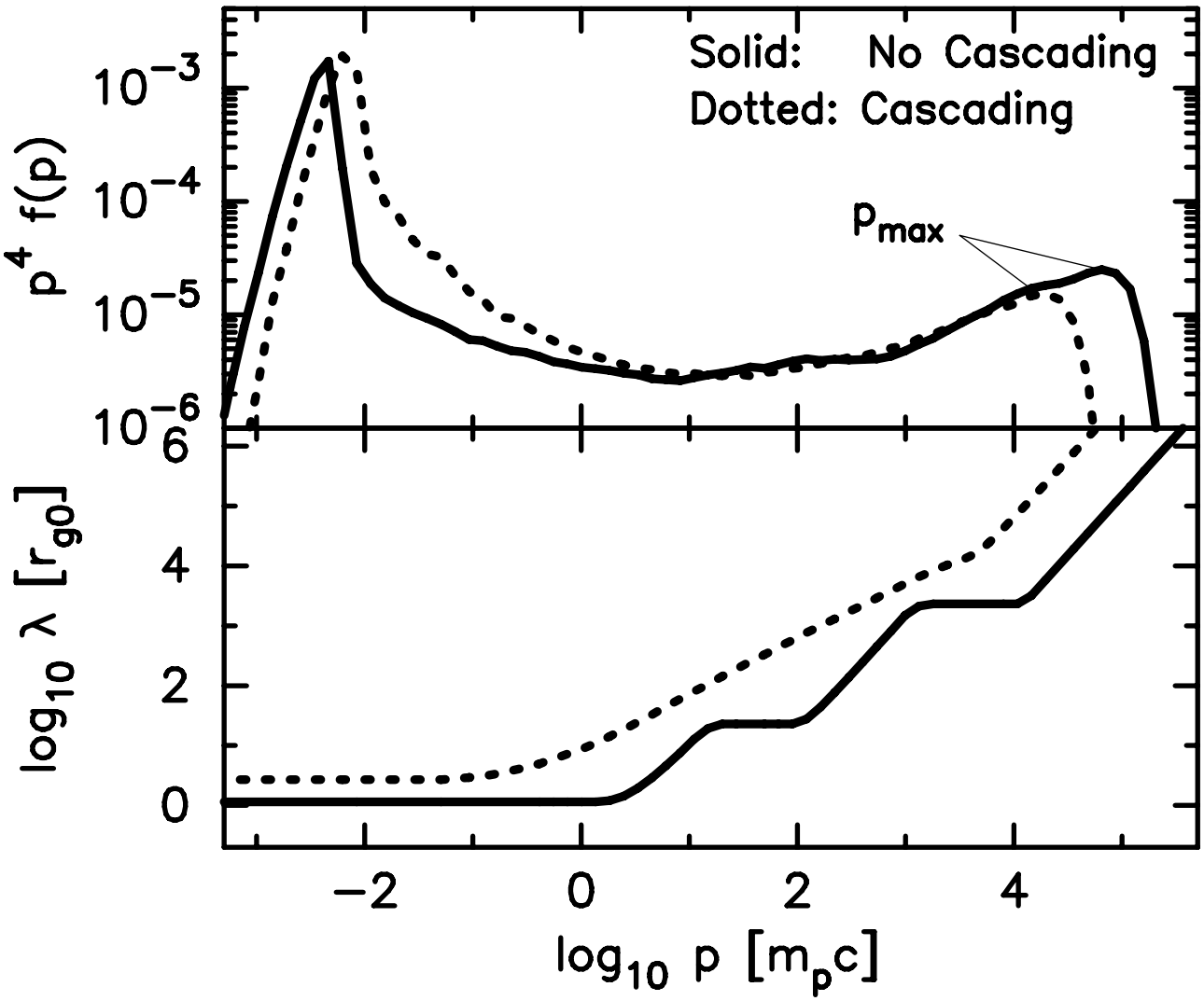

MC model of DSA

How the turbulence dissipation may change the flow and particle spectra?

Self-Consistent Simulations

- Here shock structure and injection are determined self-consistently (momentum and energy are conserved).

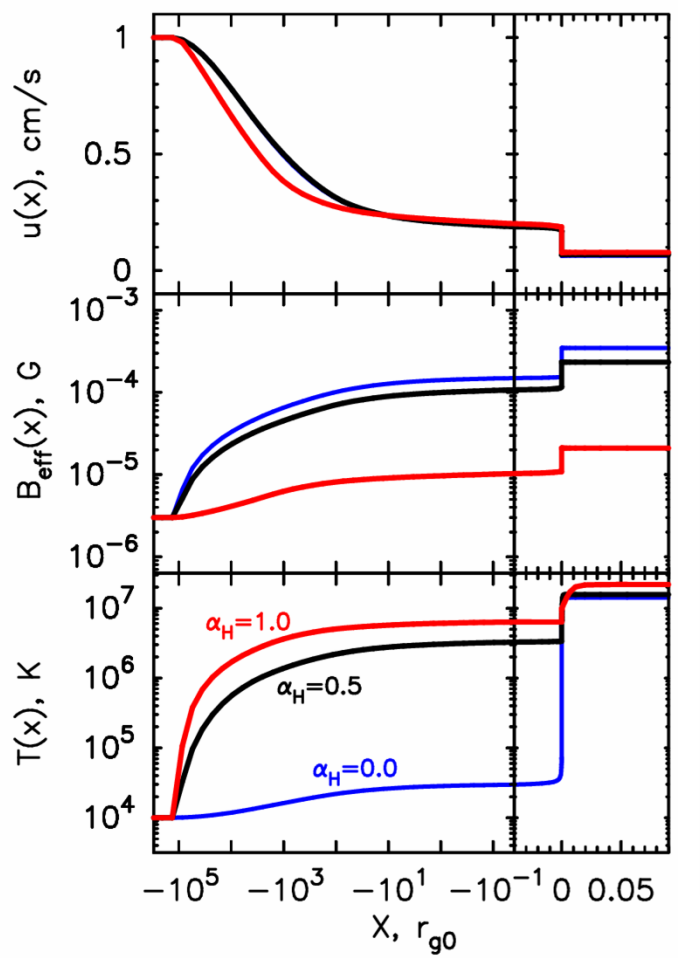

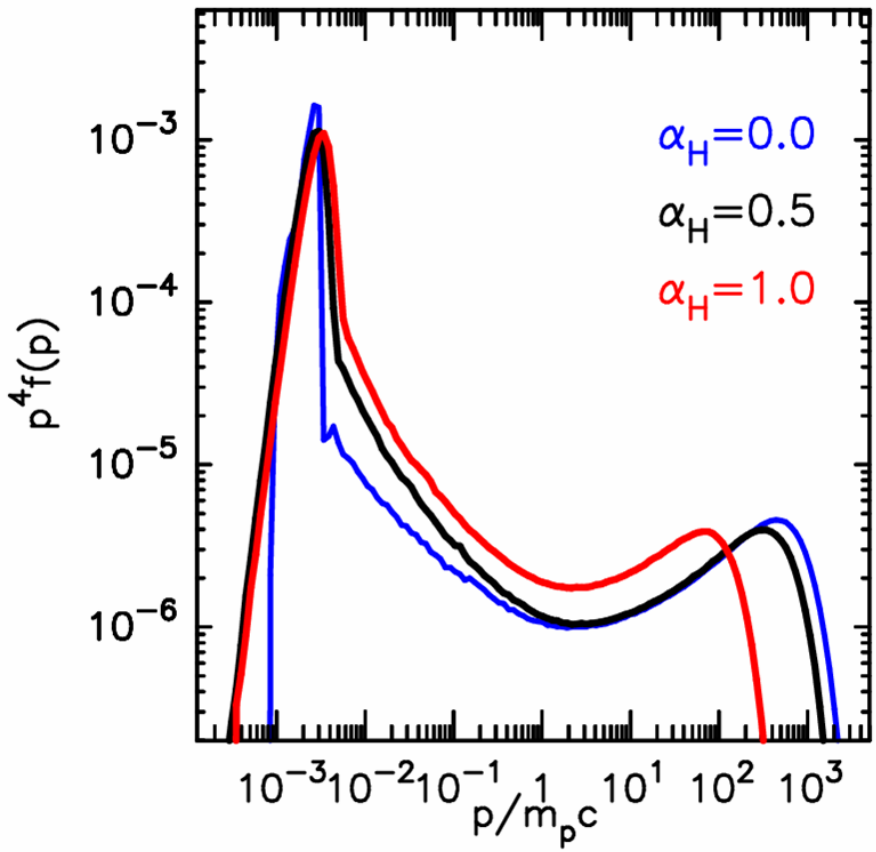

Vladimirov Bykov Ellison 2008

Optical and UV absorption and emission spectra and the line shapes are the natural tools to constrain the magnetic field dissipation in the shock upstream

What about synchrotron?

Efficient DSA requires strong magnetic turbulence with stochastic m-field amplitude above the regular m-field in the shock upstream

How that stochastic field affects the X-ray synchrotron emission?

Work done with D.C.Ellison and Yu.A.Uvarov

Bykov, Uvarov & Ellison, 2008. ApJ, v. 689, L133

Synchrotron Radiation:

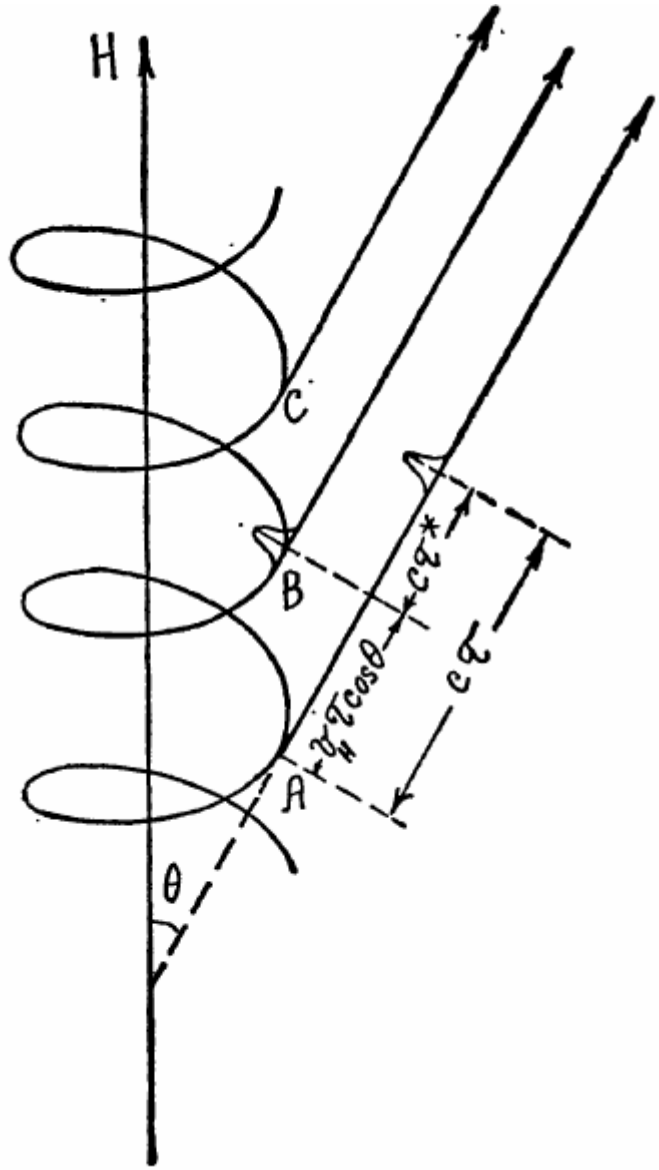

Ginzburg and Syrovatskii 1969

Synchrotron Radiation formation length:

$$l_f = \frac{R_g}{\gamma} = \frac{mc^2}{eB} \approx 1.8 \times 10^9 \; B_{\mu G}{}^{-1} [cm]$$

Field fluctuations of scales larger than l_f ***can be treated as a locally homogeneous field***

Synchrotron Radiation:

$$\mathcal{E}_n = \frac{2e\omega_H}{\sqrt{3}\,\pi c r}\,\frac{n}{\sin^5\theta}\left\{l_1(\xi^2+\psi^2)K_{2/3}(g_n) + il_2\psi(\xi^2+\psi^2)^{1/2}K_{1/3}(g_n)\right\}$$

where

$$g_n = n\,\frac{(\xi^2+\psi^2)^{3/2}}{3\sin^3\theta} = \frac{\nu}{2\nu_c}\left(1+\frac{\psi^2}{\xi^2}\right)^{3/2}, \qquad \nu = \frac{n\omega_H}{2\pi\sin^2\theta}$$

$$\nu_c = \frac{3\omega_H\sin\theta}{4\pi\xi^3} = \frac{3eH_\perp}{4\pi mc}\left(\frac{E}{mc^2}\right)^2$$

Ginzburg Syrovatskii 1969

Synchrotron Radiation Stockes Parameters:

From this and from expressions 2.18, 2.22 we can find the spectral density of the radiation flux for the two main directions of polarization

$$\tilde{p}_\nu^{(1)} \equiv \tilde{p}_{11}(\nu) = \frac{3e^2\omega_H}{4\pi^2 r^2 c\xi^2 \sin^2\theta}\left(\frac{\nu}{\nu_c}\right)^2\left(1+\frac{\psi^2}{\xi^2}\right)^2 K_{2/3}^2(g_\nu) \qquad 2.25$$

$$\tilde{p}_\nu^{(2)} \equiv \tilde{p}_{22}(\nu) = \frac{3e^2\omega_H}{4\pi^2 r^2 c\xi^2 \sin^2\theta}\left(\frac{\nu}{\nu_c}\right)^2\frac{\psi^2}{\xi^2}\left(1+\frac{\psi^2}{\xi^2}\right) K_{1/3}^2(g_\nu) \qquad 2.26$$

Ginzburg and Syrovatskii 1969

Synchrotron Radiation Stockes Parameters:

$$\hat{\tilde{S}} = \begin{pmatrix} \tilde{I}(\mathbf{r},t,\nu) \\ \tilde{Q}(\mathbf{r},t,\nu) \\ \tilde{U}(\mathbf{r},t,\nu) \\ \tilde{V}(\mathbf{r},t,\nu) \end{pmatrix} = \begin{pmatrix} p_\nu^{(1)} + p_\nu^{(2)} \\ (p_\nu^{(1)} - p_\nu^{(2)}) \cdot \cos 2\chi \\ (p_\nu^{(1)} - p_\nu^{(2)}) \cdot \sin 2\chi \\ (p_\nu^{(1)} - p_\nu^{(2)}) \cdot \tan 2\beta \end{pmatrix}$$

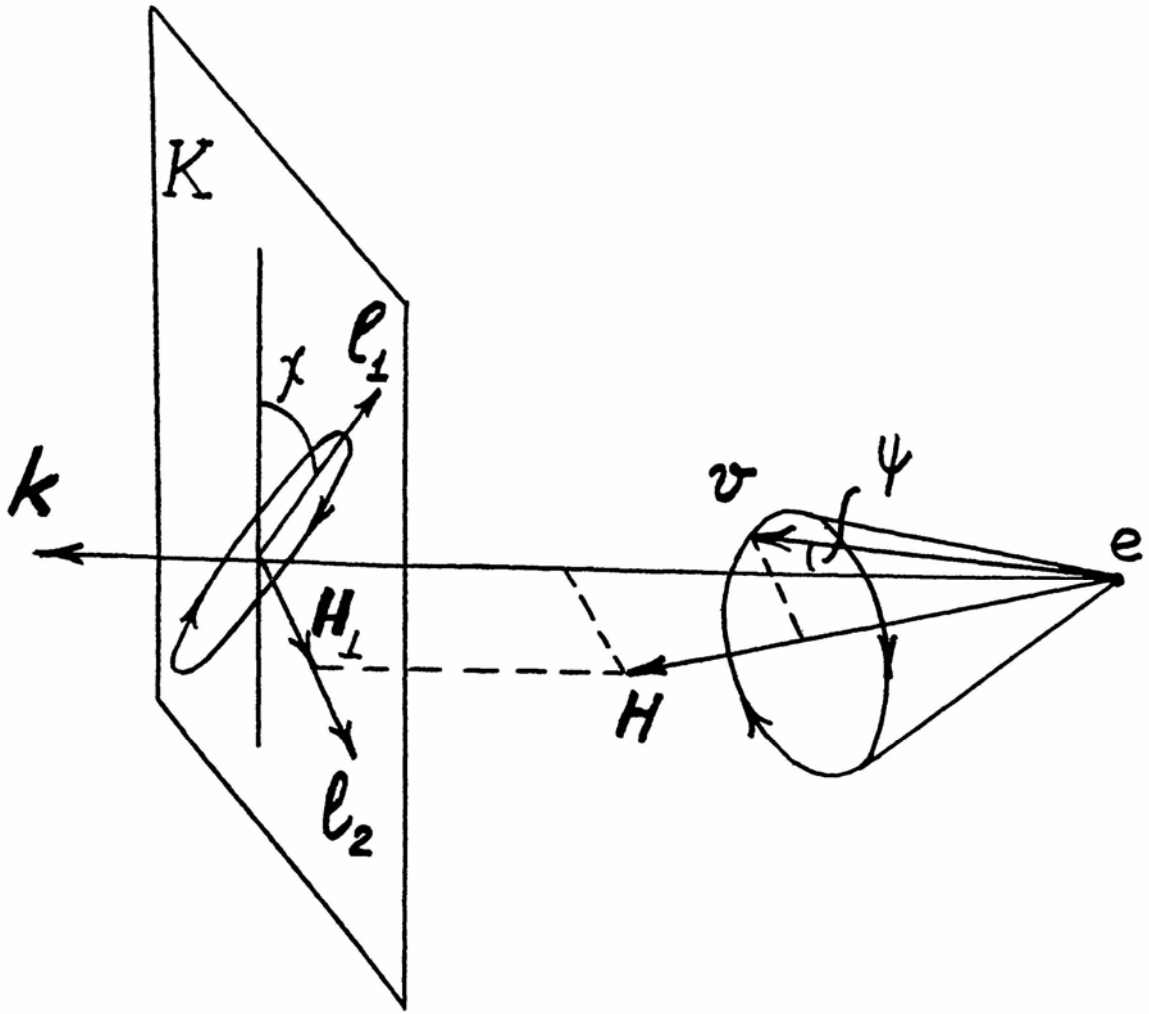

FIG. 5. Oscillation ellipse of the electric vector in a wave radiated by particles moving in a magnetic field, where the charge is taken as a positive. For negatively charged particles (electrons) the direction of rotation is opposite to that shown. The plane K is the plane of the figure (the plane perpendicular to the direction of the radiation or, equivalently, to the direction of the observer), and l_1 and l_2 are two mutually orthogonal unit vectors in the plane of the figure, of which l_2 is directed along the projection of the magnetic field H on the plane K.

Local Synchrotron Emissivity for a power-law electron distribution:

$$I_{syn}(\nu,\mathbf{r}) \sim N_e \cdot (B\sin\chi)^{(\alpha+1)/2} \cdot \nu^{-(\alpha-1)/2}$$

$$N(\gamma) = N_e \cdot \gamma^{-\alpha}$$

Note the strong dependence of the emissivity I on B

in the spectral cut-off regime !

Because of the strong dependence of the emissivity I on B in the cut-off spectral regime a strong local magnetic field enchancement could even dominate integral over the line of sight…

High statistical moments of the magnetic field distribution are important… intermittency

Synchrotron Radiation Stockes Parameters:

$$\hat{S}(\mathbf{R}_\perp, t, \nu) = \int dl\, d\gamma\, N(\mathbf{r}, \gamma, t')\, \hat{\tilde{S}}(\mathbf{r}, t', \nu, \gamma), \quad t' = t - |\mathbf{r} - \mathbf{R}_\perp|/c.$$

- Electron Distribution Simulated with Kinetic Model

Ele

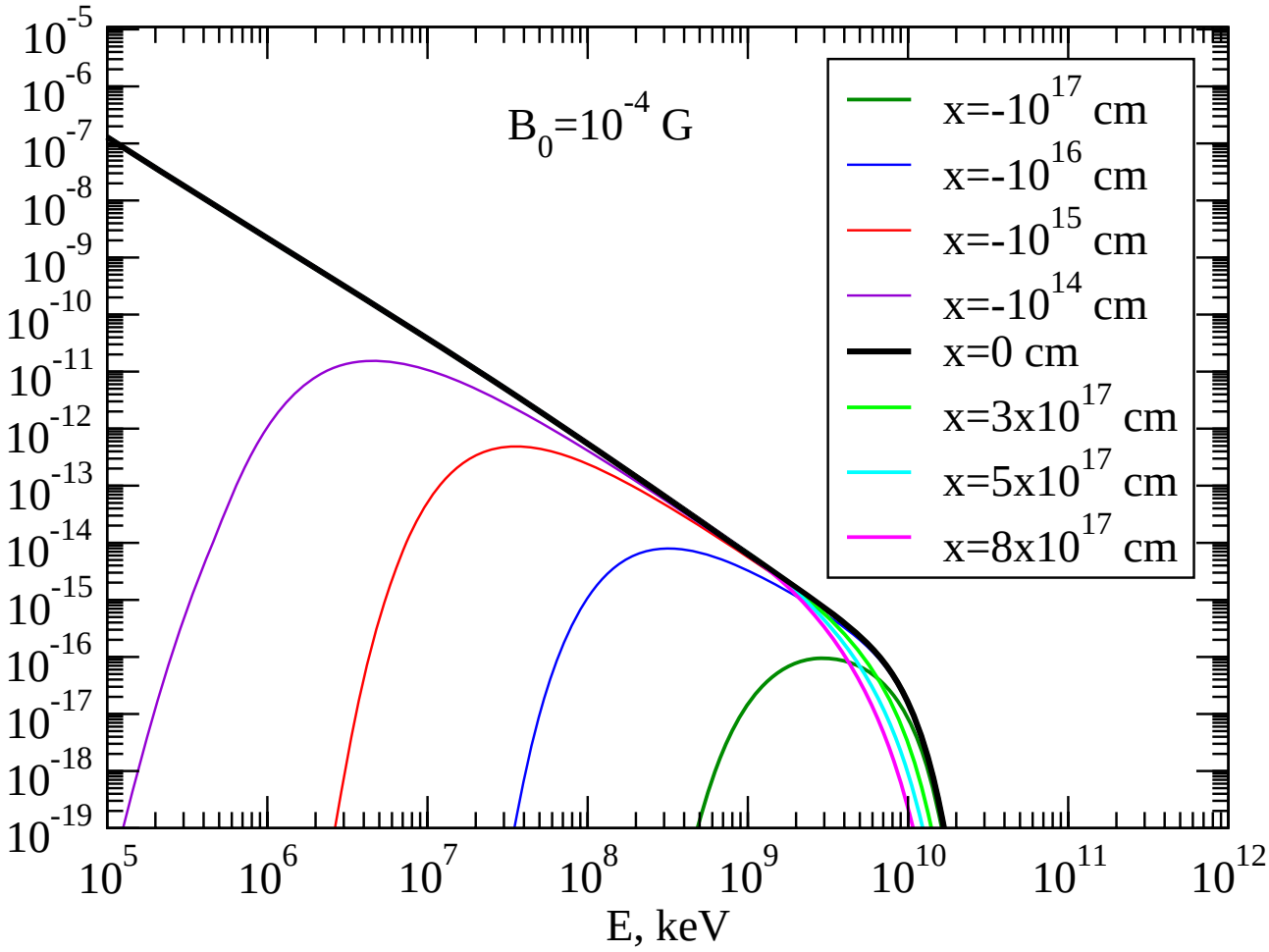
B0=10-4 G
x=-10^17 cm
x=-10^16 cm
x=-10^15 cm
x=-10^14 cm
x=0 cm
x=3x10^17 cm
x=5x10^17 cm
x=8x10^17 cm
E, keV

- A model of stochastic magnetic field

We just simulated random magnetic fields with given fluctuation spectra in four decade wave-number band

Random magnetic field generation prescription:

$$\mathbf{B}(\mathbf{r},t) = \sum_{n=1}^{N_m} \sum_{\alpha=1}^{2} \mathbf{A}^{(\alpha)}(k_n) \cos(\mathbf{k}_n \cdot \mathbf{r} - \omega_n(\mathbf{k}_n) \cdot t + \phi_n^{(\alpha)}) \ , \qquad (1)$$

where the two orthogonal polarizations $\mathbf{A}^{(\alpha)}(k_n)$ $(\alpha = 1, 2)$ are in the plane perpendicular to the wave vector direction (i.e., $\mathbf{A}^{(\alpha)}(k_n) \perp \mathbf{k}_n$, so as to ensure that $\nabla \cdot \mathbf{B} = 0$). We divided k-space between $k_{\min} = 2\pi/L_{\max}$ and $k_{\max} = 2\pi/L_{\min}$ into N spherical shells distributed uniformly on a logarithmic scale (a number of points in the s-shell is M_s). Here $L_{\min}$ and $L_{\max}$ are the minimum and maximum scales of turbulence respectively. The spectral energy density of the magnetic field fluctuations is taken as $W(k) \propto k^{-\delta}$, where δ is the spectral index.

$$\langle B^2 \rangle = \int dk \, W(k)$$

The average square magnetic field $\langle B^2 \rangle$ is an input parameter for our model. In the particular

- Synchrotron Emission Images and Spectra

Synchrotron Emission Images

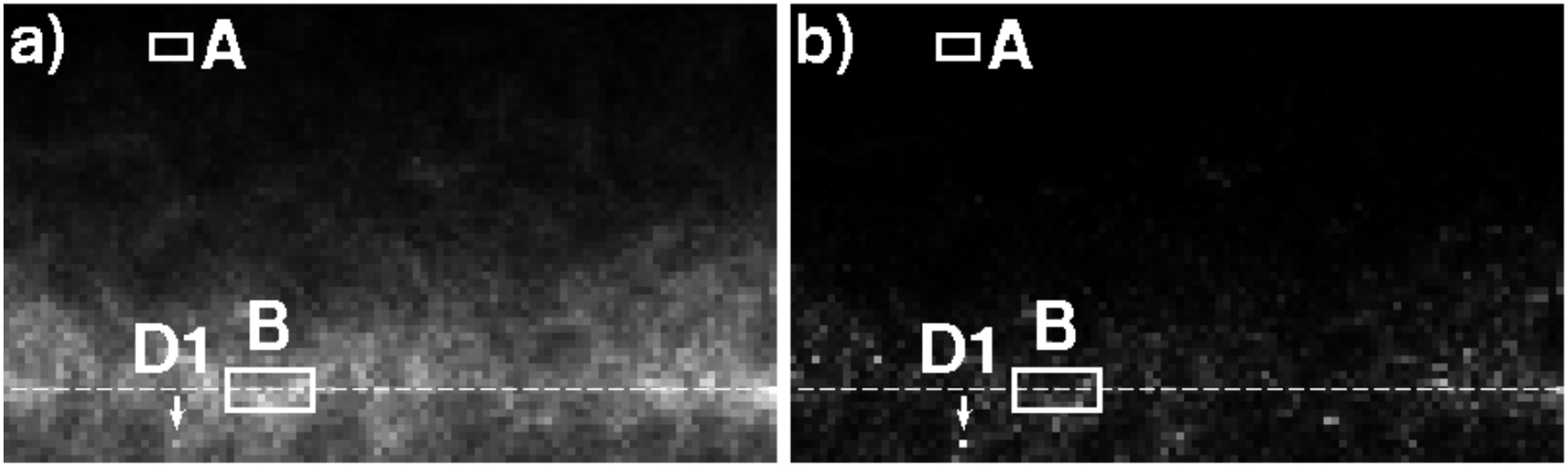

Synchrotron Emission Images (Zoom)

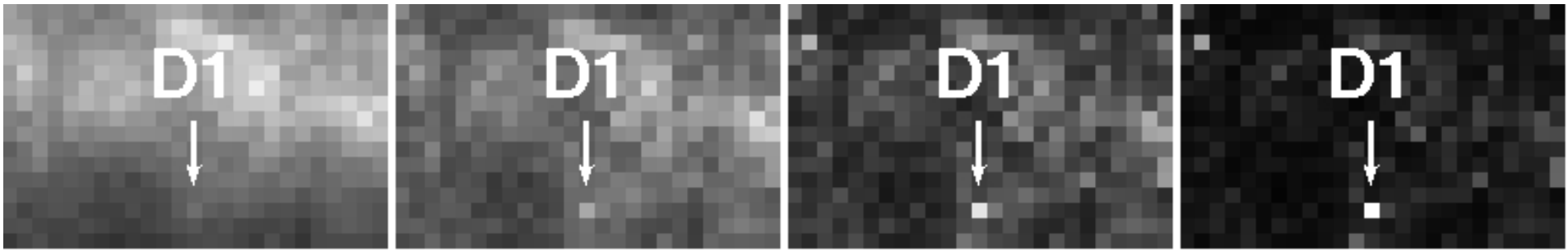

0.5 keV 5 keV 20 keV 50 keV

BUE 2008

Light Curves for Clump D1

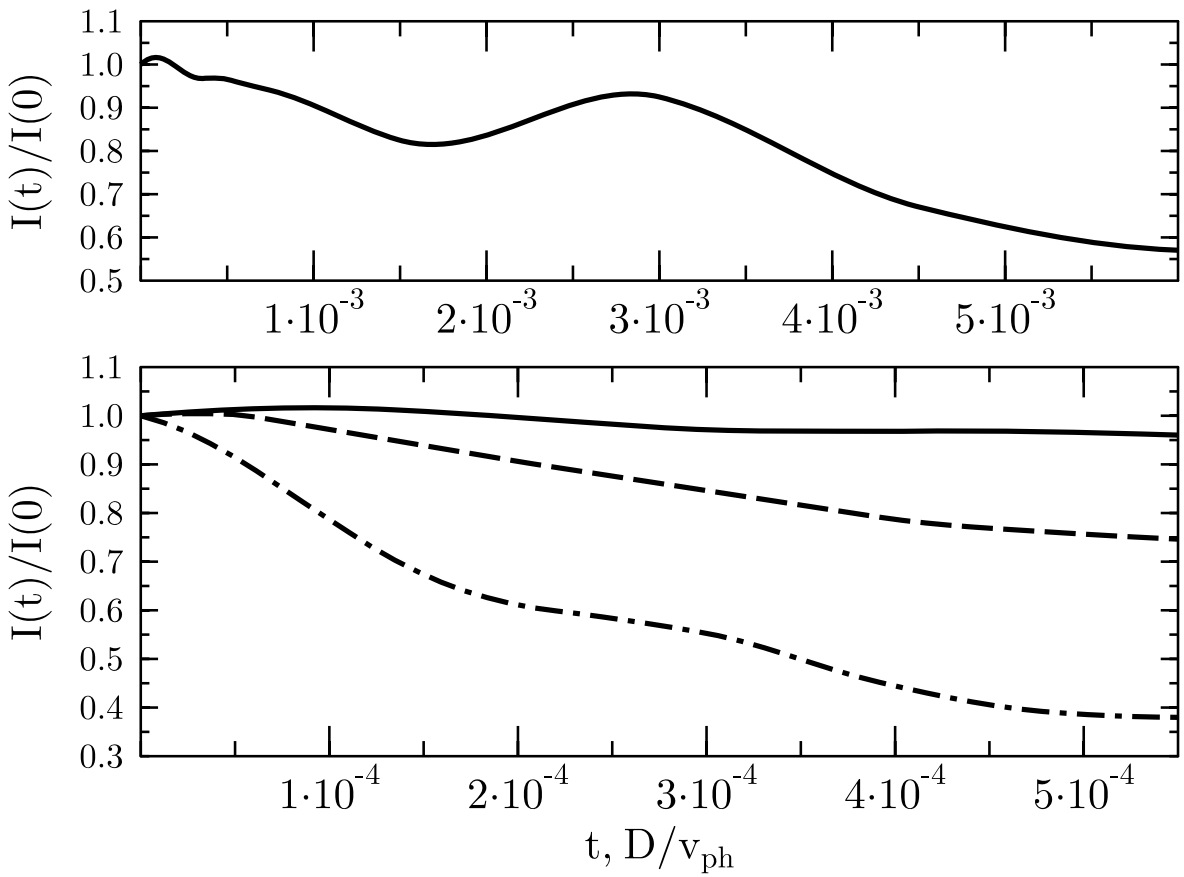

Synchrotron Emission Spectra

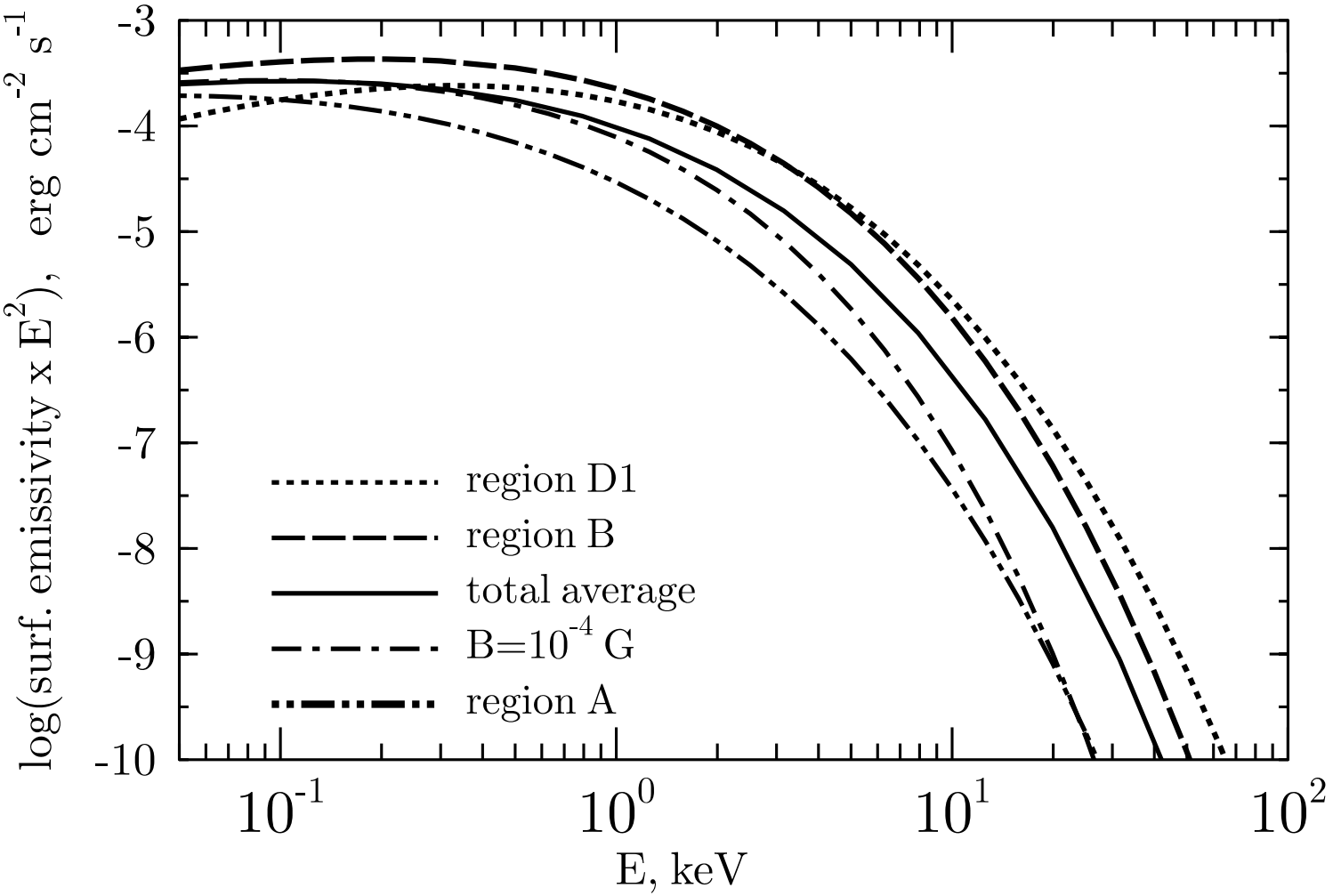

BUE 2008

The account for magnetic field magnitude fluctuations (not just the random field directions, as it was done before) result in a very strong enchancement of synchrotron surface brightness in the cut-off spectral regime.

The effect should be accounted for in the models that are making the turbulent magnetic fields estimations using the roll-off frequency…

Time variability of simulated synchrotron X-ray image at 5keV

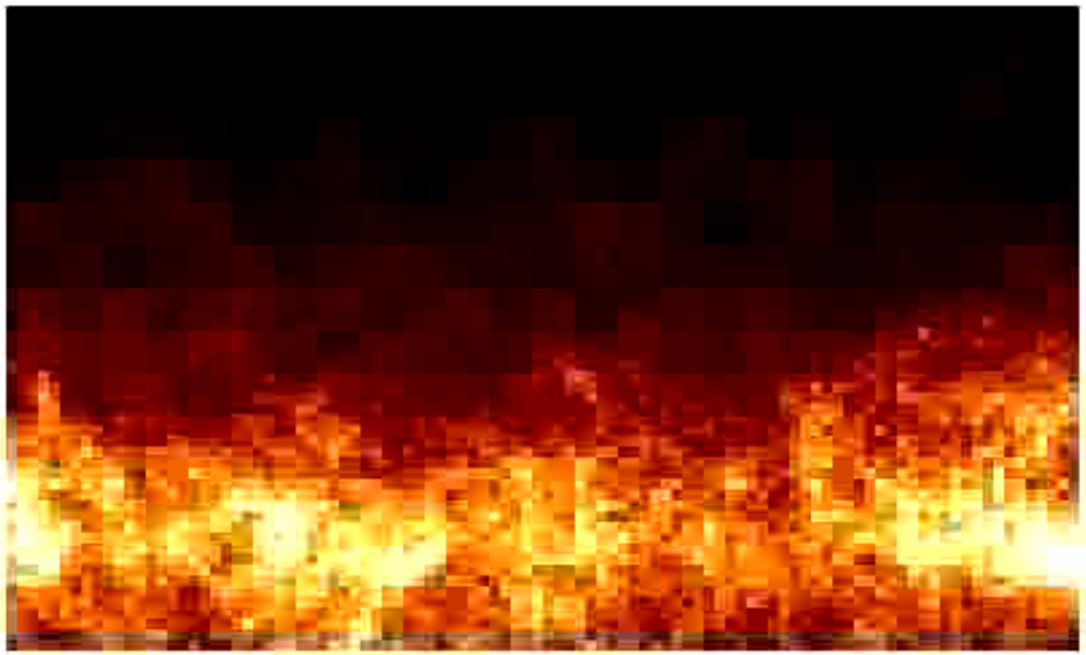

Bykov Uvarov Ellison 2008

Simulated synchrotron X-ray image @ 50 keV

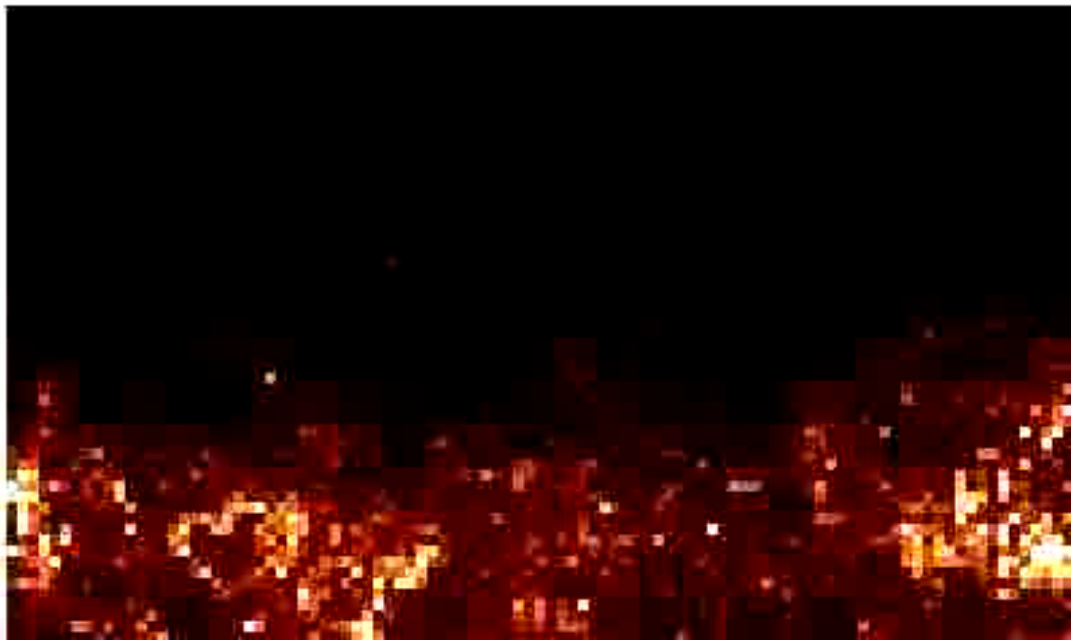

Bykov Uvarov Ellison 2008

- Variability time scale is below a year

Synchrotron Images for different turbulence spectra

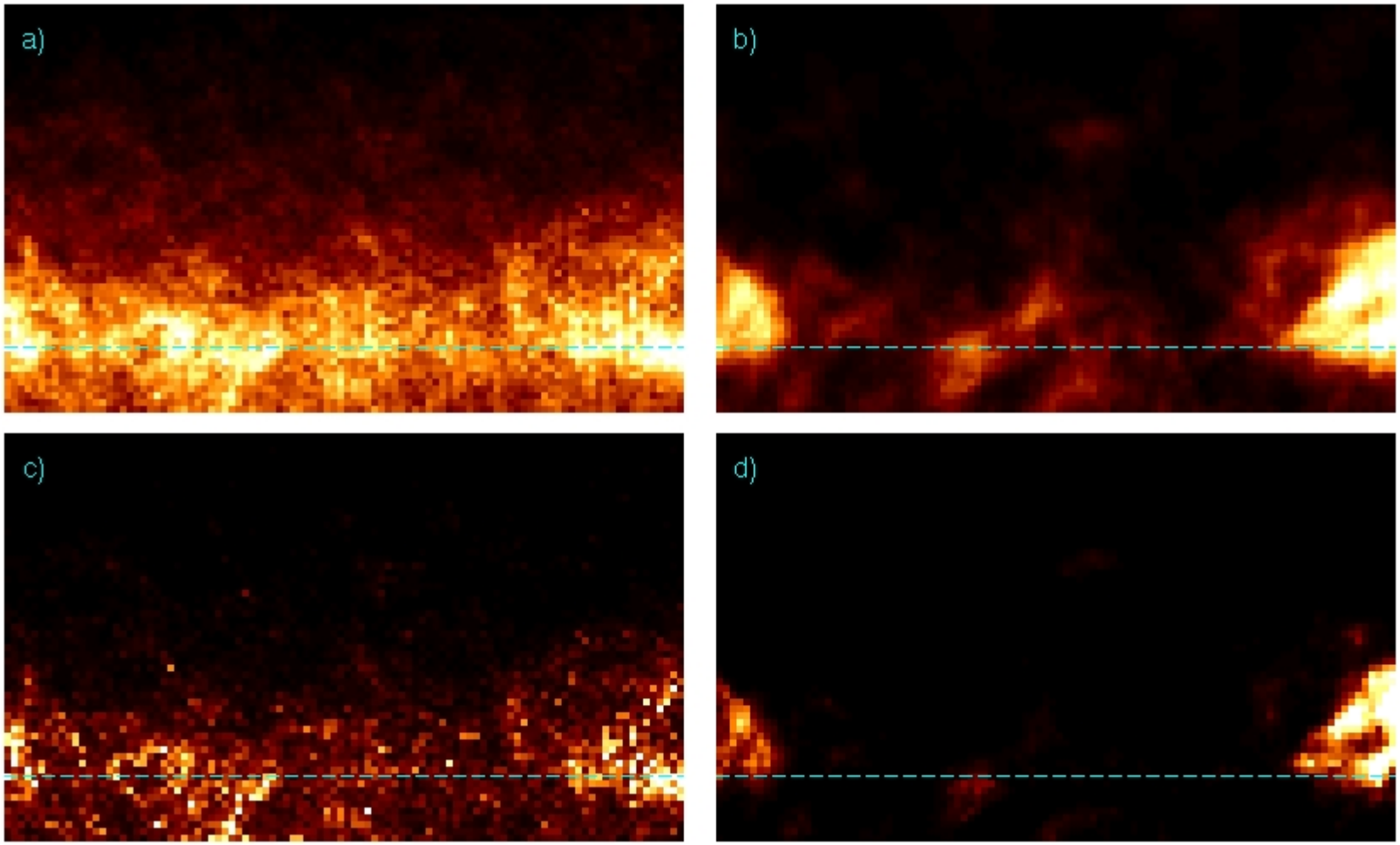

Chandra imag of RXJ1713 NW

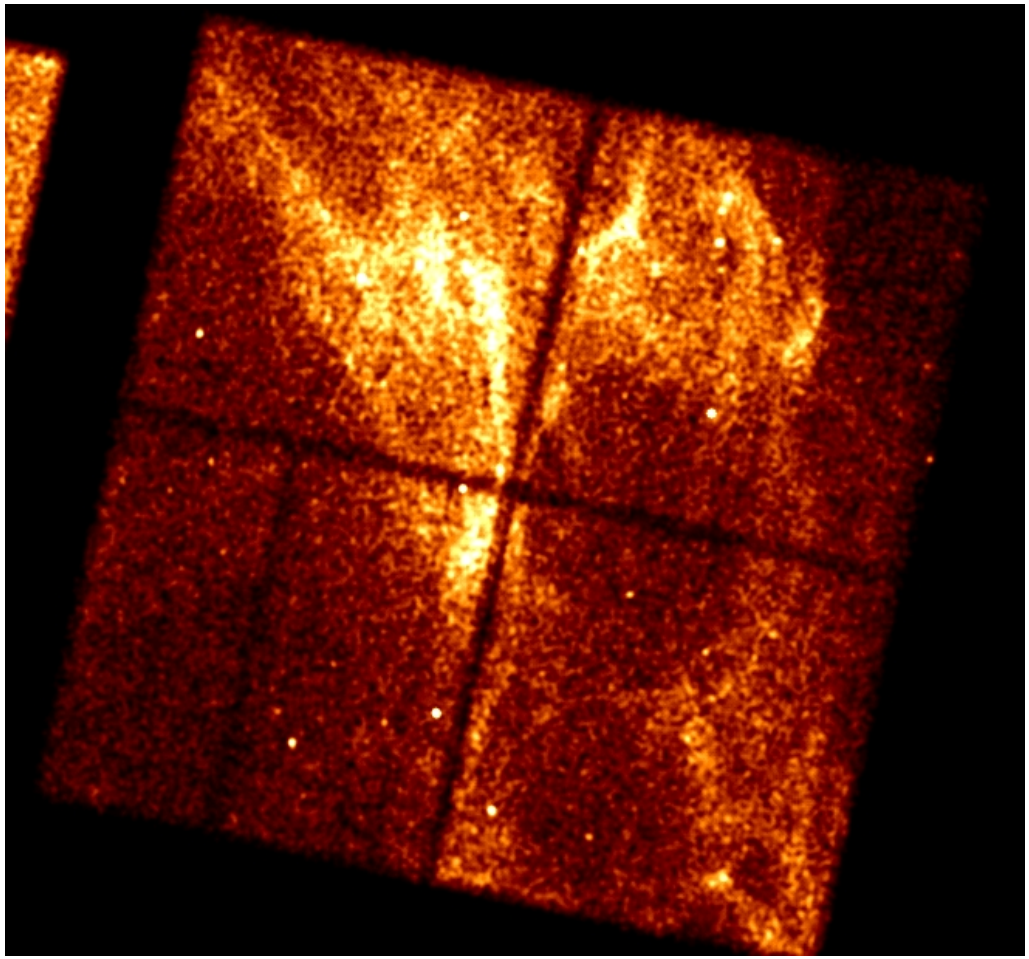

- ***RX J1713.7-3946***

Uchiyama et al. 2007

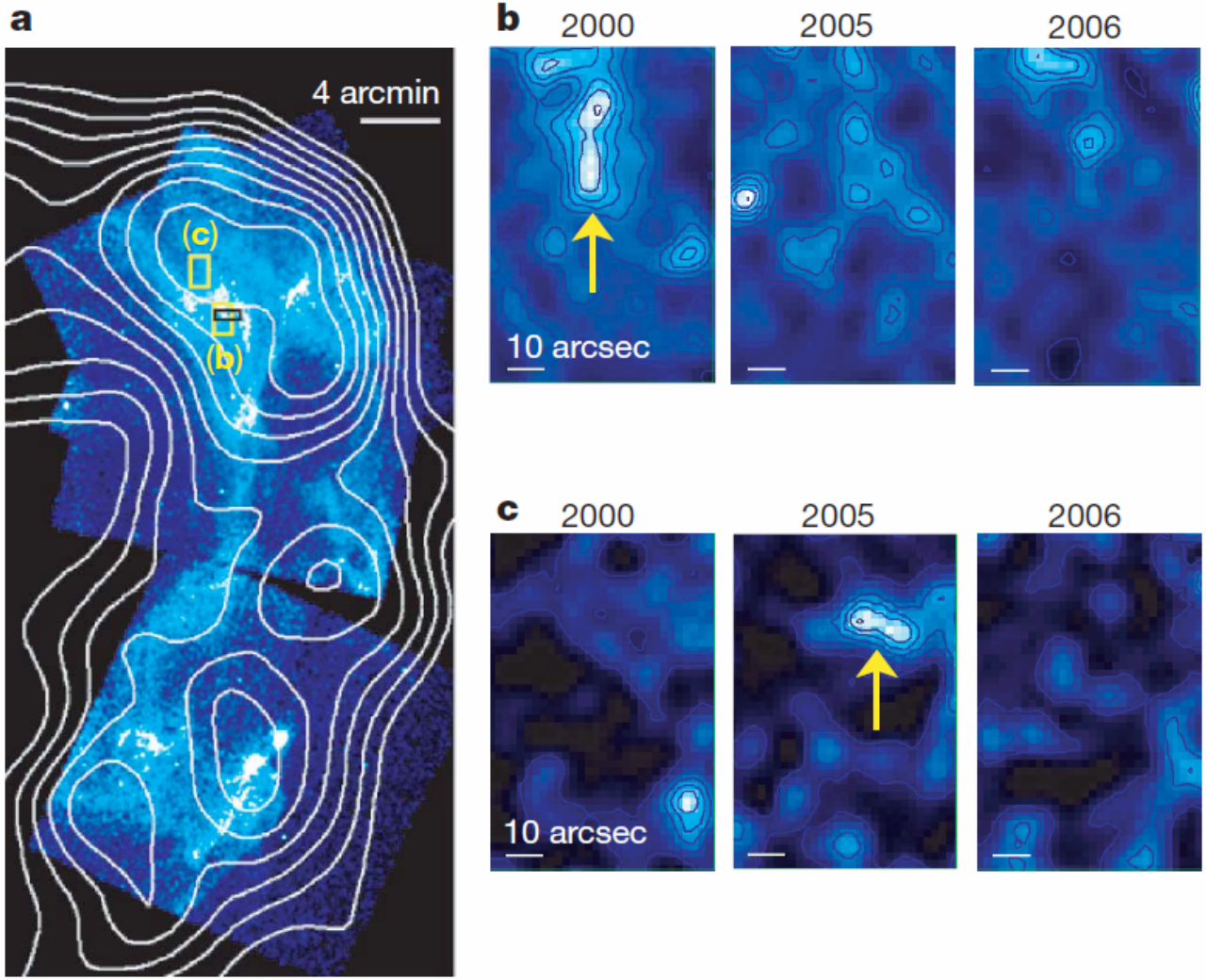

Nonthermal clump "lifetime" ~ 1yr !!

RX J1713.73946

Uchiyama et al. 2007, Nature, 449, 576

$$t_{\rm synch} \approx 1.5\,(B/{\rm mG})^{-1.5}\ (\varepsilon/{\rm keV})^{-0.5}\ {\rm years}$$

Synch. cooling time ~ 1yr result in high ~ mG regime magnetic field??

Extremely fast acceleration of cosmic rays in a supernova remnant ***???***

- ***RX J1713.7-3946***

Uchiyama et al. 2007

nature Vol 449|4 October 2007|doi:10.1038/nature06210

LETTERS

Extremely fast acceleration of cosmic rays in a supernova remnant

Yasunobu Uchiyama[1], Felix A. Aharonian[2,3], Takaaki Tanaka[1,4], Tadayuki Takahashi[1] & Yoshitomo Maeda[1]

SN 1006 Suzaku

The roll-off energy, $\nu_{\rm roll}$, is described as

$$\nu_{\rm roll} = 1.6 \times 10^{16} \left(\frac{B}{10\ \mu{\rm G}} \right) \left(\frac{E_{\rm e}}{10\ {\rm TeV}} \right)^2 , \qquad (1)$$

where $E_{\rm e}$ and B represent the maximum energy of accelerated electrons and the magnetic field strength, respectively (Reynolds 1998; Reynolds & Keohane 1999). The maximum energy of electrons is estimated to be 9.4 TeV, under the assumption that the downstream magnetic field strength is 40 μG. The time scale of the synchrotron loss, $\tau_{\rm loss}$, is

Bamba e.a. 2008

RX J1713.73946

Uchiyama et al. 2007, Nature, 449, 576

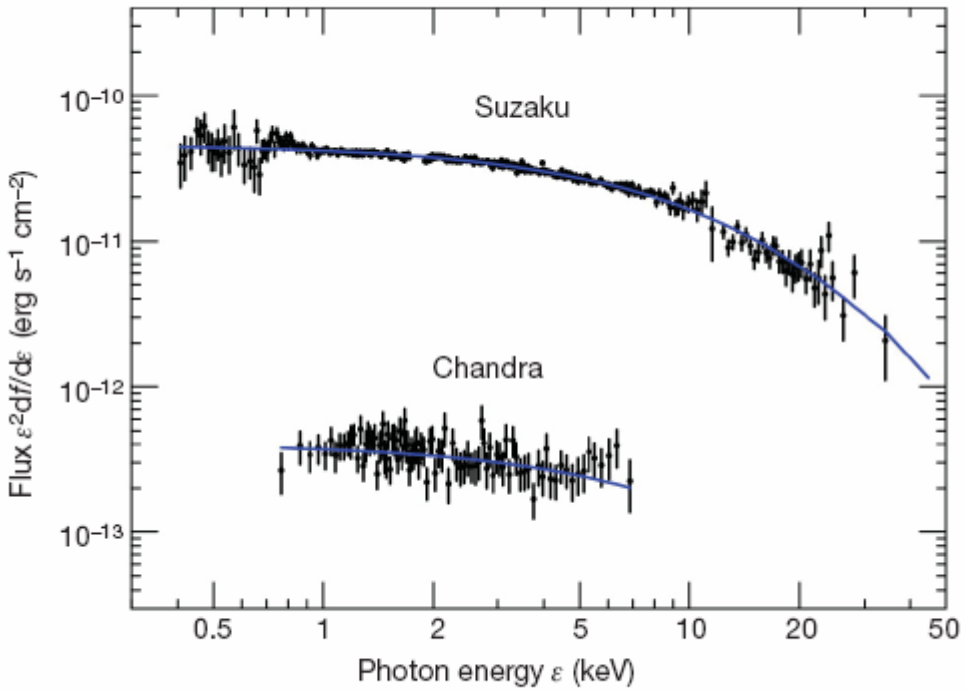

Figure 3 | Energy spectrum of X-ray emission of SNR RX J1713.7−3946.

RX J1713.7-3946

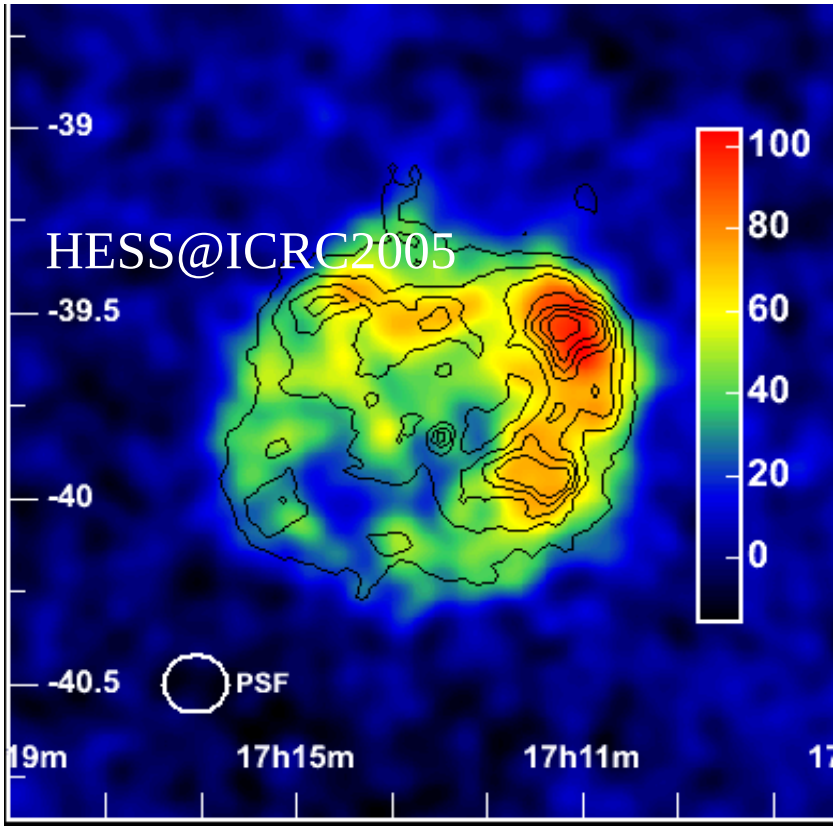

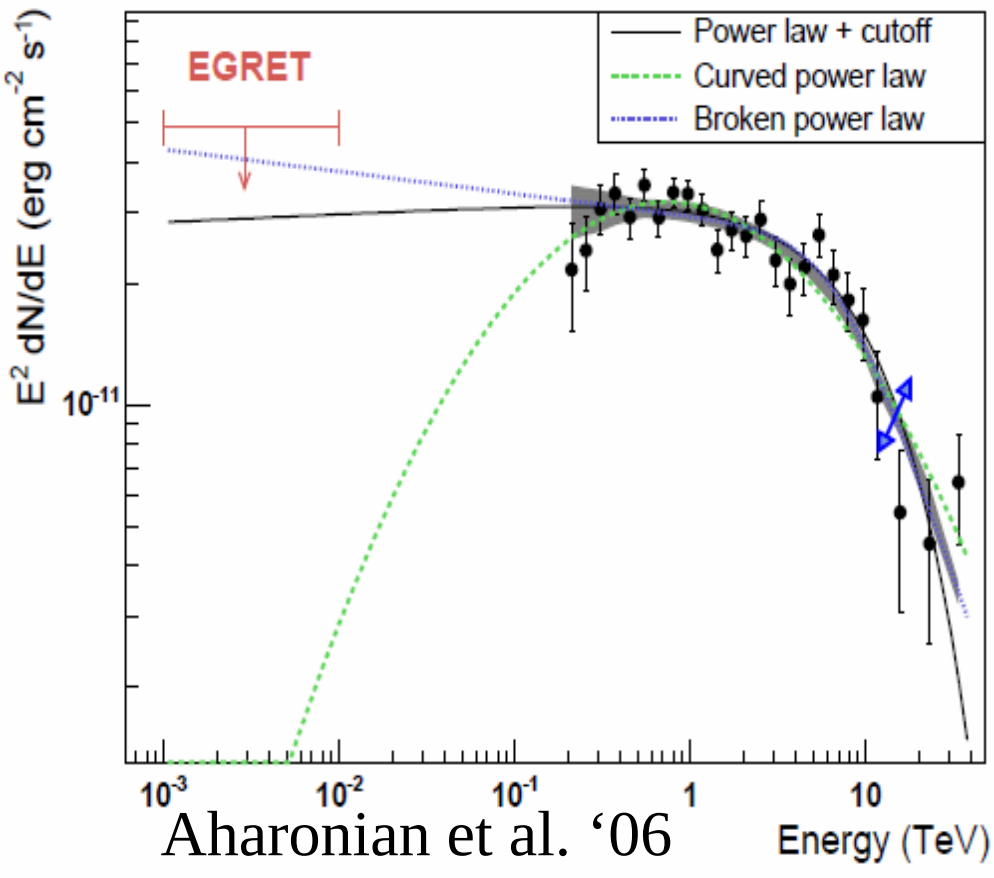

Aharonian et al. '06

Cas A

Likely Synchrotron X-ray structures that are seen in Cas A:
filaments (Vink & Laming (2003)
clumps and dots (Uchiyama & Aharonian (2008), Patnaude & Fesen (2008, 2009) could be relevant to DSA and the turbulent magnetic field amplification processes